Spectral response of magnetically trapped Bose gases to weak microwave fields

P. Federsel, C. Rogulj, T. Menold, J. Fortágh, and A. Günther*

Physikalisches Institut der Universität Tübingen, Auf der Morgenstelle 14, D-72076 Tübingen, Germany

(Received 29 May 2015; published 1 September 2015)

Microwave fields can be used to drive local spin transitions in quantum gases and for outcoupling of cold atomic beams from magnetic traps. In this paper, we derive an analytic theory for the outcoupling rate as a response to weak microwave fields of varying frequency and power. The theory holds for thermal clouds and Bose-Einstein condensates. It allows for calculating transition rates in arbitrary magnetic trap geometries and includes the effect of gravity. We verify our theory by measuring the flux of outcoupled atoms at the single-particle level. The derived spectral response is important for magnetic noise spectroscopy with quantum gases, and for probing quantum gas dynamics with single atom detectors in real time.

DOI: 10.1103/PhysRevA.92.033601 PACS number(s): 03.75.Pp, 07.77.−n, 67.85.−d

I. INTRODUCTION

Radio-frequency and microwave fields driving atomic spin and hyperfine transitions are commonly used for extracting ultracold atoms from magnetic traps. Coherent atom laser beams are obtained from Bose-Einstein condensates (BECs) by applying weak radio-frequency and microwave radiation [1–6], magnetic field noise is measured through atom loss from magnetic traps [7–10], and the dynamics of magnetized cantilevers [11] or current driven beams [12] may be measured through the detection of spin flipped atoms. For the modeling and analysis of such systems, the knowledge of the spectral response of the magnetically trapped gas is necessary, which has been calculated so far only for Bose-Einstein condensates in harmonic trap geometries [13–18]. Here we elaborate the model of the spectral response of thermal and condensed Bose gases trapped in arbitrary magnetic potentials in the presence of gravity.

In particular, we investigate the response of magnetically trapped Bose gases to microwave radiation resonant with atomic spin or hyperfine transitions. Our study focuses on the weak-coupling regime, where the number of outcoupled atoms is small and typically not detectable by standard imaging methods but by single atom counting [19–22]. Using a quasiclassical approach, we derive an analytic expression for the outcoupling rate and its frequency dependence and find that outcoupling from thermal clouds and Bose-Einstein condensates follows the same integral equation. We validate our model by measuring the spectral response of thermal atomic clouds and Bose-Einstein condensates.

II. QUASICLASSICAL THEORY OF THE SPECTRAL RESPONSE

The interaction of a magnetically trapped gas of atoms with a microwave field is illustrated in Fig. 1(a). We take the example of thermal and Bose-condensed clouds of ^{87}Rb atoms corresponding to our experiments described in this paper. Initially the atoms are magnetically trapped in a low-field seeking spin state. The microwave radiation drives a transition to a nontrapped spin state. Spin-flipped atoms leave the trap. We calculate the outcoupling rate as a function of the microwave frequency, i.e., the spectral response of the atomic cloud.

A. Resonance condition and resonance surface

In general, the microwave field couples two hyperfine states $|F,m_F\rangle \leftrightarrow |F',m_{F'}\rangle$ with energies directly connected to the magnetic trapping potential,

$$U_{F,m_F} = g_F \mu_B m_F |\vec{B}| =: U_{\mathrm{mag}}, \tag{1}$$

$$U_{F',m_{F'}} = g_{F'} \mu_B m_{F'} |\vec{B}| = \frac{g_{F'} m_{F'}}{g_F m_F} U_{\mathrm{mag}}. \tag{2}$$

Here we assume the atoms to be initially prepared in the trapped $|F,m_F\rangle$ state. The resonance condition then requires

$$\hbar\omega_{\mathrm{res}} \stackrel{!}{=} \Delta U = U_{\mathrm{mag}} \left(1 - \frac{g_{F'} m_{F'}}{g_F m_F}\right) \tag{3}$$

with $\omega_{\mathrm{res}} = \omega_{mw} - \omega_0$ being the magnetic-field oscillation frequency with respect to the zero-field transition frequency ω_0 [see Fig. 1(a)]. Defining the dimensionless parameter λ,

$$\lambda = \left(1 - \frac{g_{F'} m_{F'}}{g_F m_F}\right)^{-1}, \tag{4}$$

which amounts to $\lambda = 2/3$ in the case of Fig. 1, the resonance condition reads

$$U_{\mathrm{mag}}(\vec{r}_{\mathrm{res}}) = \lambda \hbar \omega_{\mathrm{res}}. \tag{5}$$

The manifold of points $\{\vec{r}_{\mathrm{res}}\}$ for which Eq. (5) is fulfilled defines the resonance surface, which for a given microwave frequency is given by the equipotential surface of the magnetic potential. Outside this surface atoms are detuned from the resonance by

$$\delta(\vec{r}) = \omega(\vec{r}) - \omega_{\mathrm{res}} = \frac{U_{\mathrm{mag}}(\vec{r})}{\lambda\hbar} - \omega_{\mathrm{res}} \tag{6}$$

with $\omega(\vec{r}) = U_{\mathrm{mag}}(\vec{r})/\lambda\hbar$ being the position dependent frequency at which $\vec{r}$ is coupled resonantly [cf. Fig. 1(b)].

B. Outcoupling from thermal clouds

We calculate the outcoupling rate of thermal atoms, which are steadily moving in the trap, using a Landau-Zener model

*a.guenther@uni-tuebingen.de

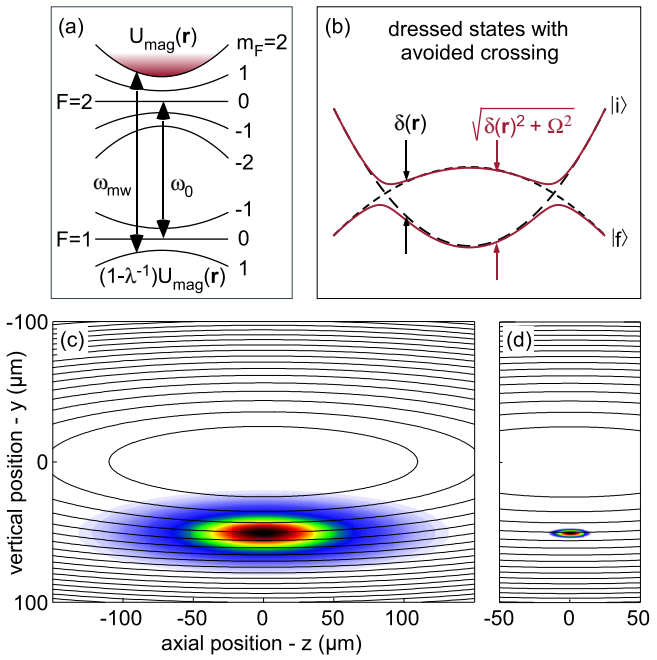

FIG. 1. (Color online) Microwave outcoupling of ^{87}Rb atoms. (a) Outcoupling scheme: Atoms are initially prepared in the $5S_{1/2}$, $|F=2, m_F=2\rangle$ state ($g_F=1/2$), where they are trapped in a magnetic potential $U_{\rm mag}(\vec{r})$. Energy selective outcoupling is achieved by microwave (mw) coupling to the nontrapped $|F=1, m_F=1\rangle$ state ($g_F=-1/2$). The coupling rate depends strongly on the intensity and frequency of the applied microwave and allows for tomographic investigation of quantum gases. (b) Dressed state picture for mw coupling of the initial and final bare states, $|i\rangle$ and $|f\rangle$. The microwave coupling causes degeneracy at the resonance positions and a spatial dependent detuning (black dashed line). Due to the coupling strength the dressed state energies change slightly (red line), resulting in avoided crossings at the resonance positions. (c),(d) Microwave resonance surfaces and density distributions for a thermal cloud of 190 nK (c) and a BEC of 8000 atoms (d) in a harmonic trap with $\omega_{x/y/z} = 2\pi \times 85,\ 70,\ 16$ Hz. Resonance surfaces are shown for microwave frequency spacings of $2\pi \times 20$ kHz. They are elliptically shaped and centered around the magnetic field minimum. Both density distributions are displaced by the gravitational sag, amounting to $y_0 \approx 50\ \mu$m. For small cloud extensions (BEC), the resonance surfaces can be approximated as flat.

for the spin transitions. For particles crossing the resonance surface the probability of a state transfer is given by [23]

$$P_0 = 1 - \exp\left(-\frac{\pi\Omega^2}{2|\alpha|}\right) \approx \frac{\pi\Omega^2}{2|\alpha|} \tag{7}$$

with α being the change of detuning over time,

$$\alpha = \frac{d\delta(\vec{r})}{dt} = \frac{d\omega(\vec{r})}{dt} = \frac{\vec{\nabla}U_{\rm mag}\cdot\vec{v}}{\partial U_{\rm mag}/\partial\omega} = \frac{\vec{\nabla}U_{\rm mag}\cdot\vec{v}}{\lambda\hbar}, \tag{8}$$

and Ω being the resonant Rabi frequency, which we assume to be constant across the cloud. This assumption holds for typical experimental conditions [24]. The local crossing rate of particles with velocity $\vec{v}$ through a resonance surface element dA amounts to

$$\gamma_v = n(\vec{r})\,\vec{v}\cdot d\vec{A} \tag{9}$$

with $d\vec{A} \parallel \vec{\nabla}U_{\rm mag}$ oriented normal to the resonance surface. The local outcoupling rate $d\Gamma_v = P_0 \times \gamma_v$ is thus velocity independent and the total rate becomes

$$\Gamma = \int d\Gamma_v = \frac{\pi\Omega^2\lambda\hbar}{2}\oint \frac{n(\vec{r})\,dA}{|\vec{\nabla}U_{\rm mag}|}, \tag{10}$$

where the integral has to be evaluated on the resonance surface.

C. Outcoupling from Bose-Einstein condensates

For condensates we use a different approach, where the microwave coupling induces local Rabi oscillations, resulting in an outcoupled atomic density [14]

$$n_{\rm out}(\vec{r},t) = \frac{\Omega^2 \sin^2\left(\frac{1}{2}\sqrt{\delta(\vec{r})^2+\Omega^2}\,t\right)}{\delta(\vec{r})^2+\Omega^2} n(\vec{r}). \tag{11}$$

The outcoupling rate then amounts to

$$\Gamma(t) = \frac{d}{dt}\int n_{\rm out}(\vec{r},t)dV \tag{12}$$

$$= \frac{\Omega^2}{2}\int \frac{\sin\left(\sqrt{\delta^2+\Omega^2}\,t\right)}{\sqrt{\delta^2+\Omega^2}} n(\vec{r})dV. \tag{13}$$

Changing the base to curvilinear coordinates, with one base vector given by $d\vec{r}/d\omega$ and the others spanning the resonance surface element dA, results in a transformation

$$dV = \frac{dU_{\rm mag}/d\omega}{|\vec{\nabla}U_{\rm mag}|} d\omega dA = \frac{\lambda\hbar}{|\vec{\nabla}U_{\rm mag}|} d\omega dA. \tag{14}$$

After substituting $\tilde{\omega} = \omega - \omega_{\rm res}$, the outcoupling rate becomes

$$\Gamma(t) = \frac{\Omega^2\lambda\hbar}{2} \underbrace{\int_{-\infty}^{\infty} d\omega \frac{\sin\left(\sqrt{\tilde{\omega}^2+\Omega^2}\,t\right)}{\sqrt{\tilde{\omega}^2+\Omega^2}}}_{\pi J_0(\Omega t)} \oint dA \frac{n(\vec{r})}{|\vec{\nabla}U_{\rm mag}|}. \tag{15}$$

Here we have used that the main contribution to the transition rate comes from the resonance shell of width $\delta\omega \approx \Omega \ll \omega_{\rm res}$, corresponding to a spatial width δy much smaller than the BEC extension, such that the ω integral can be extended to $-\infty$ and $n(\vec{r})/|\vec{\nabla}U_{\rm mag}|$ approximated by its resonance value. The ω integral can then be solved by means of Bessel functions [14].

The remaining time dependence in the outcoupling rate of Eq. (15) is due to resonant backcoupling of outcoupled atoms, which, at least for low Rabi frequencies, is strongly suppressed by the outcoupled atoms falling out of the resonance shell. The dynamics of Eq. (15) is thus only valid at $t = 0$, where all atoms remain trapped. The total loss rate then becomes

$$\Gamma = \frac{\pi\Omega^2\lambda\hbar}{2}\oint \frac{n(\vec{r})dA}{|\vec{\nabla}U_{\rm mag}|}, \tag{16}$$

which is identical to the expression found for thermal clouds.

D. Numeric and analytic solutions

Evaluating the resonance surface integral in Eq. (16) is typically nontrivial, especially if a proper surface parametrization is missing. However, using the vector identity $dA = (d\vec{A}\cdot\vec{\nabla}U_{\rm mag})/|\vec{\nabla}U_{\rm mag}|$ and the divergence theorem,

the surface integral can be rewritten as a volume integral

$$\oint \frac{n(\vec{r})}{|\vec{\nabla}U_{\mathrm{mag}}|} dA = \int \mathrm{div}\left(\frac{n(\vec{r})}{|\vec{\nabla}U_{\mathrm{mag}}|^2}\vec{\nabla}U_{\mathrm{mag}}\right) dV, \quad (17)$$

which is easily solved numerically. Here, the integral has to be evaluated in the volume enclosed by the resonance surface.

Nevertheless, certain trap geometries allow for a proper parametrization of the resonance surface. This especially holds for harmonic potentials with trap frequencies ω_x, ω_y, ω_z, as found in almost all Ioffe-type field configurations close to the trap center. Figures 1(c) and 1(d) show the ellipsoidal resonance surfaces in such a situation, alongside density distributions for a typical thermal cloud and a BEC. Using scaled spherical coordinates ($a \geqslant 0, \theta \in [0,\pi], \varphi \in [0,2\pi]$), with transformation rules

$$\begin{aligned} x &= a/\omega_x \sin\theta\cos\varphi, \\ y &= a/\omega_y \sin\theta\sin\varphi, \\ z &= a/\omega_z \cos\theta, \end{aligned} \quad (18)$$

the magnetic potential reads

$$U_{\mathrm{mag}} = \sum_{i=1}^{3} \frac{1}{2} m\omega_i^2 x_i^2 = \frac{1}{2} m a^2 \equiv \lambda\hbar\omega \quad (19)$$

and solely depends on the coordinate a. The resonance surfaces, given by the equipotential surface of U_{mag}, are thus well parametrized by φ and θ and Eq. (16) transforms to

$$\Gamma = \frac{\pi\Omega^2\lambda\hbar}{2} \frac{a}{m\omega_x\omega_y\omega_z} \iint n(\vec{r}) \sin\theta d\theta d\varphi. \quad (20)$$

Taking gravity into account, the density distribution of thermal clouds and BECs both depend on the total atomic potential $U = U_{\mathrm{mag}} - mgy$. While still being harmonic, the total potential minimum is shifted to $y_0 = g/\omega_y^2$, known as gravitational sag, and energetically lowered by $U_0 = mg^2/(2\omega_y^2)$ [see Figs. 1(c) and 1(d)]. Following Boltzmann distribution, the density of a thermal cloud reads

$$n_{th}(\vec{r}) = n_0 \exp\left(-\frac{\lambda\hbar\omega}{k_B T}\right) \exp\left(\frac{mga\sin\theta\sin\varphi}{\omega_y k_B T}\right) \quad (21)$$

with n_0 given by normalization to the total atom number N. Using this density distribution Eq. (20) can be solved analytically yielding

$$\Gamma_{th}(\omega) = \frac{\pi\Omega^2\lambda\hbar}{2} \frac{N}{\sqrt{\pi U_0 k_B T}} \exp\left(-\frac{U_0 + \lambda\hbar\omega}{k_B T}\right) \times \sinh\left(2\sqrt{\frac{U_0}{k_B T}\frac{\lambda\hbar\omega}{k_B T}}\right). \quad (22)$$

For sufficient small cloud extensions as in the case of BECs, the outcoupling surface can be approximated by a plane surface [see Fig. 1(d)], yielding the resonance condition

$$\frac{1}{2} m\omega_y^2 y^2 = \lambda\hbar\omega \quad \rightarrow \quad y(\omega) = \sqrt{\frac{2\lambda\hbar\omega}{m\omega_y^2}}. \quad (23)$$

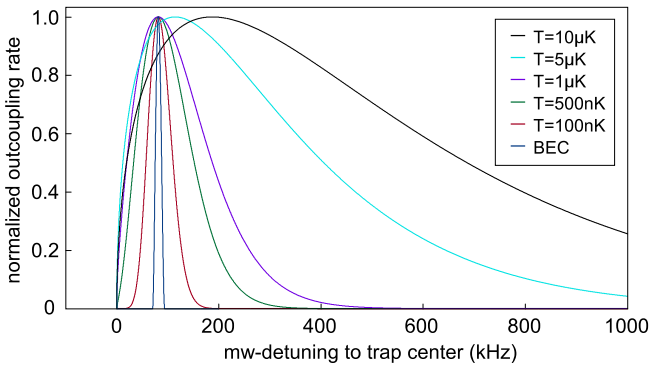

FIG. 2. (Color online) Spectral response of thermal clouds and a BEC with 10 000 atoms in a harmonic trap with trapping frequencies $\omega_{x/y/z} = 2\pi \times 85,\ 70,\ 16$ Hz, as calculated from Eqs. (22) and (24). For $T > 1\ \mu$K the spectral shape is dominated by the cloud temperature, giving access to the particles' energy distribution. For $T < 1\ \mu$K the spectral response depends directly on the cloud's density profile and the gravitational acceleration, allowing for spatial tomography of quantum gases.

With $|\vec{\nabla}U_{\mathrm{mag}}| \approx m\omega_y^2 y$ the integral in Eq. (16) can be solved in Cartesian coordinates yielding

$$\Gamma(\omega) = \frac{\pi\Omega^2}{2} \sqrt{\frac{\lambda\hbar}{2m\omega_y^2}} \frac{n[y(\omega)]}{\sqrt{\omega}} \quad (24)$$

with $n(y) = \iint n dx dz$ being the integrated line density. For a BEC in the Thomas-Fermi limit, this line density is given by

$$n_{\mathrm{bec}}(y) = \frac{\mu\pi R_x R_z}{2g} \max\left[0, 1 - \frac{(y-y_0)^2}{R_y^2}\right]^2 \quad (25)$$

with the coupling strength $g = 4\pi\hbar^2 a/m$, the scattering length a, the Thomas Fermi radii $R_i = \sqrt{2\mu/(m\omega_i^2)}$ and the chemical potential μ given via normalization.

E. Discussion

Following Eq. (16), the total outcoupling rate scales quadratically with the Rabi frequency and thus linearly with the microwave power density. This is expected in the weak-coupling regime, where saturation effects and Rabi oscillations are negligible. Figure 2 shows the spectral response, as calculated from Eqs. (22) and (24), for thermal clouds of different temperatures and Bose-Einstein condensates. For the calculations we used a harmonic trap geometry with trapping frequencies $\omega_{x/y/z} = 2\pi \times 85,\ 70,\ 16$ Hz, as in the experimental section of this paper.

For large cloud extensions, $\Delta y \gg y_0$, the gravitational sag is negligible and the outcoupling rate from Eq. (22) becomes

$$\Gamma \sim \sqrt{\omega} \exp\left(-\frac{\lambda\hbar\omega}{k_B T}\right). \quad (26)$$

The maximum ω_0 and width $\Delta\omega$ (full width at half maximum) of the spectral response are then given by the cloud temperature only:

$$\omega_0 \approx k_B T/2\lambda\hbar, \quad \Delta\omega \approx 1.8 k_B T/\lambda\hbar, \quad (27)$$

as illustrated by the $T > 1\ \mu$K curves in Fig. 2. In this regime, the spectral response yields mainly information about the particles' energy distribution.

For small cloud extensions, $\Delta y \ll y_0$, the gravitational sag becomes dominant and the outcoupling rate can be approximated by Eq. (24), yielding

$$\Gamma \sim \frac{n[y(\omega)]}{\sqrt{\omega}}. \tag{28}$$

In this regime, the maximum of the spectral response is shifted with respect to the magnetic-field minimum, to a value independent from the cloud temperature,

$$\lambda\hbar\omega_0 \approx \frac{1}{2}m\omega_y^2 y_0^2 \quad \rightarrow \quad \omega_0 \approx \frac{mg^2}{2\lambda\hbar\omega_y^2}, \tag{29}$$

amounting $\omega_0 = 2\pi \times 81.6$ kHz in Fig. 2. With the gradient of the magnetic potential being compensated by the gravitational force at the trap center, the spectral width of the response function is now directly connected to the spatial width Δy and the gravitational acceleration g,

$$\frac{dU_{\mathrm{mag}}}{dy} = \lambda\hbar\frac{d\omega}{dy} \approx mg \quad \rightarrow \quad \Delta\omega = \frac{mg}{\lambda\hbar}\Delta y. \tag{30}$$

We note that only in this regime does the spectral response follow directly from the spatial distribution of the atomic cloud. According to Eq. (28), the frequency-dependent outcoupling rate is then a direct measure for the cloud's spatial density profile. This gives an interesting opportunity of tomographic measurements on the quantum gas, e.g., the measurement of density variations of a spin component between resonance shells or collective oscillations of the quantum gas.

The frequency resolution $\delta\omega$ of such a mw tomography will be typically given by the width of the resonance shell, $\delta\omega \approx \Omega$, which might be additionally broadened due to the atoms' dwell time in the resonance region. This translates according to Eq. (30) to a spatial resolution $\delta y = \lambda\hbar\delta\omega/mg$, given by the thickness of the resonance sheet, which is typically in the submicrometer regime and thus much smaller than the spatial extension of the quantum gas. The ultimate resolution limit is given by the sensitivity of the detection process, which sets a lower limit to the detectable Rabi frequency. Using a sensitive single atom detection scheme, as presented in the following section, high spatial resolutions may be feasible.

We note that for small cloud extensions the spectral width of the response function is largely increased due to gravity, as the cloud is shifted from the center of the magnetic trap to stronger magnetic-field gradients (cf. Fig. 2). Especially for Bose-Einstein condensates, this results in spectral widths much larger than the chemical potential, which is the main reason for the high resolution in microwave tomography.

III. EXPERIMENT

For the experimental verification of the spectral response we prepare clouds of ^{87}Rb atoms in the $5S_{1/2}, |F = 2, m_F = 2\rangle$ state in a magnetic trap [cf. Fig. 1(a) and Ref. [25]]. The confinement at the trap center is nearly harmonic with oscillation frequencies $\omega_{x/y/z} = 2\pi \times 85, 70, 16$ Hz. Gravity is acting along the y direction. A microwave field of ~6.8 GHz frequency, driving transitions from the trapped $|F = 2, m_F = 2\rangle$ to the nontrapped $|F = 1, m_F = 1\rangle$ state, is irradiated with a helix antenna. Atoms undergoing the spin-flip transition are no longer trapped and fall under gravity. We detect these outcoupled atoms with a single atom counting scheme.

The detection process is based on state selective photoionization and subsequent ion counting [26,27]. Atoms falling out of the trap enter the photoionization volume, defined by a pair of laser beams, ~300 μm below the atomic cloud. Starting from $5S_{1/2}$, $F = 1$ the atoms are first excited to the $5D_{5/2}$, $F = 3$ state via a resonant two-photon transition at 778 nm. The transition is resonantly enhanced via the $5P_{3/2}$ state, allowing saturation at few 10-mW laser power. A fiber laser at 1064 nm is then used to ionize the atoms. To compete against the natural decay of the $5D_{5/2}$ state, we use about 4-W fiber laser power, which is not yet sufficient to saturate the transition, thus limiting the ionization efficiency [20,28]. Both lasers are positioned about 300 μm below the atomic cloud with beam waists of about 50 μm. Besides driving the ionization process, the high power fiber laser creates a strong attractive dipole potential, which focuses the falling atoms to regions of high intensity. The repulsive dipole potential of the 778-nm laser is negligible. Following the photoionization, the rubidium ions are collected with an ion optics and guided to a channel electron multiplier [27]. Ions are counted with 8-ns temporal resolution. The detection efficiency, 24%, has been calibrated by comparing the number of ions counted with the loss of atoms from the trap observed through absorption imaging. The detector's background count rate, measured without atoms but all ionization lasers and readout electronics turned on, amounts to about 1 Hz.

To verify the theoretical results found in Sec. II, we experimentally measure the response of ultracold atoms to microwave fields of varying power and frequency. After preparing a thermal cloud or Bose-Einstein condensate, we irradiate the microwave at constant or time-varying frequency for about 1 s, while monitoring the outcoupled atoms with the state selective single atom detector. Counting the atoms in 1-ms bins allows for extracting time resolved outcoupling rates, which we then compare to our theory. Trap frequencies, temperatures, and atom numbers of the atomic clouds have been derived from standard absorption imaging. The Rabi frequency has been calibrated by sweeping the microwave at a constant rate of 1.6 MHz/s through the cloud and monitoring the remaining atom fraction via absorption imaging. Comparing the result to the Landau-Zener theory from Eq. (7) allows for extracting the Rabi frequency.

A. Spectral response

In a first experiment we measure the shape of the spectral response function. We sweep the mw frequency at a constant rate of 1.3 kHz/ms, starting with a positive detuning of ~500 kHz with respect to the magnetic-field minimum. The mw power is tuned to $\Omega = 2\pi \times 84$ Hz, such that the total outcoupling losses stay below 10%. Due to the single atom sensitivity of the detector, this is sufficient to measure the full spectral response function within a single sweep. Figure 3 shows the measured response for a thermal cloud of 160 nK and a BEC at 30 nK with 8200 atoms.

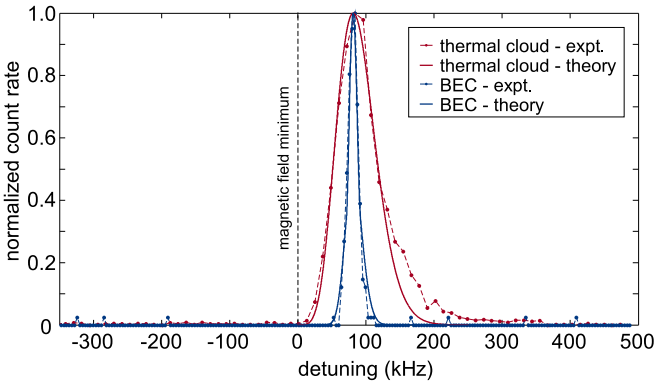

FIG. 3. (Color online) Spectral response of a thermal cloud (red points) and a BEC (blue points), measured by sweeping the mw frequency through the cloud, while detecting the ion count rate. For a single sweep through the thermal cloud ($N = 730 \times 10^3$, $T = 160$ nK) and the BEC ($N = 8200$, $T \approx 30$ nK), the total number of detected ion amounts are 4000 and 50, respectively. To reduce noise, the BEC measurement is shown as average of four sweeps. Microwave frequencies are shown relative to the magnetic trap center (black dashed line), located at 876 and 873 mG for the thermal cloud and BEC. From the measurements we deduce the FWHM (full width half maximum) of the spectral response to be 69 kHz for the thermal cloud and 18 kHz for the BEC. The results from the theoretical *ab initio* calculations following Eqs. (22) and (24) are shown as solid lines.

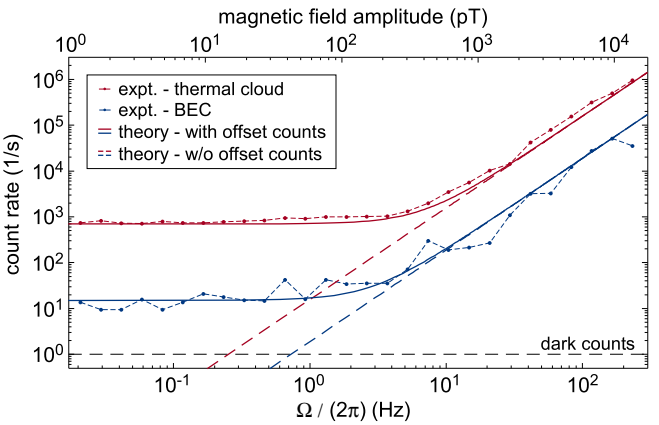

FIG. 4. (Color online) Response of a thermal cloud (red points) and a BEC (blue points) to different mw amplitudes and Rabi frequencies. At each amplitude the ion count rate is measured for 800 ms on individual clouds. Data points show the initial ionization rate as extracted from an exponential fit to the measurement time. The *ab initio* theory from Eqs. (22) and (24) is shown with zero (dashed lines) and finite (solid lines) offset count rates. The offset values for the thermal cloud ($N = 5.8 \times 10^5$, $T = 240$ nK) and the BEC ($N = 10 \times 10^3$) have been set to 700 and 15 Hz, respectively. The offset is purely technical and describes atomic spin flips driven by an off-resonant excitation from the 778-nm laser. In general (without offset) the sensitivity limit is reached at the dark count level amounting to $14.7 pT/\sqrt{\text{Hz}}$ for the thermal cloud.

The measurements are shown together with the *ab initio* calculations from Eqs. (22) and (24). Here, the finite temperature BEC is described by superimposing the response functions of a pure BEC and the corresponding thermal component. Both measurements show good agreement with the theory, with only small deviations in the high-frequency region of the thermal cloud. These deviations are due to the onset of trap anharmonicities, which could in principle be extracted from such measurements.

B. Sensitivity

In a second experiment we keep the mw frequency fixed at the maximum of the spectral response and measure the ion signal for different mw amplitudes. We stepwise increase the mw amplitude (Rabi frequency) in consecutive experimental runs ranging from $\Omega = 2\pi \times 17$ mHz up to $2\pi \times 170$ Hz. Within a single run the Rabi frequency is then fixed during the 800-ms measurement time. As for large mw powers the ion count rate may change during the measurement time; we extract the initial ionization rate by fitting an exponential function to the time resolved ionization rates. Figure 4 shows the results for a thermal cloud at 240 nK and a BEC with 10 000 atoms alongside the *ab initio* calculations from Eq. (16). For large microwave powers, we find perfect agreement and the outcoupling rate increases quadratically with the Rabi frequency. In the low power regime, however, the measured count rate saturates at values larger than the detector's background count rate. A detailed analysis shows that this offset is due to an imperfect separation of the 778-nm laser mode from the trapped atoms, causing weak optical pumping to the nontrapped $F = 1$ state. This is a purely technical effect and shall be overcome in future realizations by using a light sheet for the ionization lasers.

Using Eq. (16) and accounting for the measured 1-Hz background ion count rate we can estimate the sensitivity of magnetically trapped atomic clouds to resonant microwave radiation to be in the range $15 pT/\sqrt{\text{Hz}}$ or in terms of the Rabi frequency $2\pi \times 0.25$ Hz$/\sqrt{\text{Hz}}$.

IV. OUTLOOK

In this paper we have presented and experimentally verified a quasiclassical description for microwave outcoupling from thermal clouds and Bose-Einstein condensates in arbitrary magnetic-field configurations. Knowing the spectral response of quantum gases to radio-frequency and microwave fields will open up new perspectives for spectroscopic measurements. In future experiments weak microwave outcoupling might be used to investigate dynamical effects in quantum gases such as center of mass oscillations, collective excitations, density waves or even spin-wave dynamics. Using a sensitive single atom detector such measurements can be done at rather low Rabi frequencies, maximizing the spatial tomographic resolution. At the same time, small outcoupling rates will allow for fast data acquisition and real-time observation. Vice versa, the quantum gas might be used to characterize unknown radio-frequency or microwave fields. Besides measuring magnetic-field amplitudes down to the pT regime, such atomic quantum probes may allow local measurements of classical and quantum noise spectra close to solid-state devices.

ACKNOWLEDGMENTS

We gratefully acknowledge financial support from the DFG through SFB TRR21, the "Kompetenznetz Funktionelle Nanostrukturen" and the FET-Open Xtrack Project HAIRS. We also thank C. Zimmermann, P. Domokos, T. Kiss, and C. Vale for helpful discussions.

[1] M.-O. Mewes, M. R. Andrews, D. M. Kurn, D. S. Durfee, C. G. Townsend, and W. Ketterle, Output Coupler for Bose-Einstein Condensed Atoms, Phys. Rev. Lett. **78**, 582 (1997).

[2] I. Bloch, T. W. Hänsch, and T. Esslinger, Atom Laser with a cw Output Coupler, Phys. Rev. Lett. **82**, 3008 (1999).

[3] J. L. Martin, C. R. McKenzie, N. R. Thomas, J. C. Sharpe, D. M. Warrington, P. J. Manson, W. J. Sandle, and A. C. Wilson, Output coupling of a Bose-Einstein condensate formed in a TOP trap, J. Phys. B **32**, 3065 (1999).

[4] Y. Le Coq, J. H. Thywissen, S. A. Rangwala, F. Gerbier, S. Richard, G. Delannoy, P. Bouyer, and A. Aspect, Atom Laser Divergence, Phys. Rev. Lett. **87**, 170403 (2001).

[5] A. Öttl, S. Ritter, M. Köhl, and T. Esslinger, Hybrid apparatus for Bose-Einstein condensation and cavity quantum electrodynamics: Single atom detection in quantum degenerate gases, Rev. Sci. Instrum. **77**, 063118 (2006).

[6] N. P. Robins, P. A. Altin, J. E. Debs, and J. D. Close, Atom lasers: Production, properties and prospects for precision inertial measurement, Phys. Rep. **529**, 265 (2013).

[7] M. P. A. Jones, C. J. Vale, D. Sahagun, B. V. Hall, and E. A. Hinds, Spin Coupling between Cold Atoms and the Thermal Fluctuations of a Metal Surface, Phys. Rev. Lett. **91**, 080401 (2003).

[8] Yu-ju Lin, Igor Teper, Cheng Chin, and Vladan Vuletić, Impact of the Casimir-Polder Potential and Johnson Noise on Bose-Einstein Condensate Stability Near Surfaces, Phys. Rev. Lett. **92**, 050404 (2004).

[9] A. Emmert, A. Lupaşcu, G. Nogues, M. Brune, J.-M. Raimond, and S. Haroche, Measurement of the trapping lifetime close to a cold metallic surface on a cryogenic atom-chip, Eur. Phys. J. D **51**, 173 (2009).

[10] B. Kasch, H. Hattermann, D. Cano, T. E. Judd, S. Scheel, C. Zimmermann, R. Kleiner, D. Koelle, and J. Fortágh, Cold atoms near superconductors: Atomic spin coherence beyond the Johnson noise limit, New J. Phys. **12**, 065024 (2010).

[11] Philipp Treutlein, David Hunger, Stephan Camerer, Theodor W. Hänsch, and Jakob Reichel, Bose-Einstein Condensate Coupled to a Nanomechanical Resonator on an Atom Chip, Phys. Rev. Lett. **99**, 140403 (2007).

[12] O. Kálmán, T. Kiss, J. Fortágh, and P. Domokos, Quantum galvanometer by interfacing a vibrating nanowire and cold atoms, Nano Lett. **12**, 435 (2012).

[13] M. Holland, K. Burnett, C. Gardiner, J. I. Cirac, and P. Zoller, Theory of an atom laser, Phys. Rev. A **54**, R1757 (1996).

[14] H. Steck, M. Naraschewski, and H. Wallis, Output of a Pulsed Atom Laser, Phys. Rev. Lett. **80**, 1 (1998).

[15] J. Schneider and A. Schenzle, Output from an atom laser: Theory vs. experiment, Appl. Phys. B **69**, 353 (1999).

[16] Y. B. Band, P. S. Julienne, and M. Trippenbach, Radio-frequency output coupling of the Bose-Einstein condensate for atom lasers, Phys. Rev. A **59**, 3823 (1999).

[17] F. Gerbier, P. Bouyer, and A. Aspect, Quasicontinuous Atom Laser in the Presence of Gravity, Phys. Rev. Lett. **86**, 4729 (2001).

[18] T. Kramer and M. Rodriguez, Quantum theory of an atom laser originating from a Bose-Einstein condensate or a Fermi gas in the presence of gravity, Phys. Rev. A **74**, 013611 (2006).

[19] A. Öttl, S. Ritter, M. Köhl, and T. Esslinger, Correlations and Counting Statistics of an Atom Laser, Phys. Rev. Lett. **95**, 090404 (2005).

[20] A. Günther, H. Bender, A. Stibor, J. Fortágh, and C. Zimmermann, Observing quantum gases in real time: Single-atom detection on a chip, Phys. Rev. A **80**, 011604 (2009).

[21] R. Bücker, A. Perrin, S. Manz, T. Betz, Ch. Koller, T. Plisson, J. Rottmann, T. Schumm, and J. Schmiedmayer, Single-particle-sensitive imaging of freely propagating ultracold atoms, New J. Phys. **11**, 103039 (2009).

[22] W. S. Bakr, J. I. Gillen, A. Peng, S. Fölling, and M. Greiner, A quantum gas microscope for detecting single atoms in a Hubbard-regime optical lattice, Nature (London) **462**, 74 (2009).

[23] C. Zener, Non-adiabatic crossing of energy levels, Proc. R. Soc. London, Ser. A **137**, 696 (1932).

[24] Considering the transition illustrated in Fig. 1(a), a cloud of 10-μK temperature, and a circular polarized microwave radiated along the direction of a 1-G offset field, the Rabi frequency varies less than 7% across the cloud. The variation stays within this boundary even in the limit of large trap frequencies. In the case of Fig. 1(c) ($T = 190$ nK), the variation is less than 1.1%.

[25] A. Günther, M. Kemmler, S. Kraft, C. J. Vale, C. Zimmermann, and J. Fortágh, Combined chips for atom optics, Phys. Rev. A **71**, 063619 (2005).

[26] S. Kraft, A. Günther, J. Fortágh, and C. Zimmermann, Spatially resolved photoionization of ultracold atoms on an atom chip, Phys. Rev. A **75**, 063605 (2007).

[27] A. Stibor, H. Bender, S. Kühnhold, J. Fortágh, C. Zimmermann, and A. Günther, Single-atom detection on a chip: From realization to application, New J. Phys. **12**, 065034 (2010).

[28] A. Stibor, S. Kraft, T. Campey, D. Komma, A. Günther, J. Fortágh, C. J. Vale, H. Rubinsztein-Dunlop, and C. Zimmermann, Calibration of a single-atom detector for atomic microchips, Phys. Rev. A **76**, 033614 (2007).